Available online at www.sciencedirect.com

ScienceDirect

Procedia CIRP 137 (2025) 176–180

www.elsevier.com/locate/procedia

CIRP Conference on Electro Physical and Chemical Engineering

Pulsed Cold Spray System for Physical Unclonable Function Generation

Changheon Han[a], Ted Gabor[a], Hojun Lee[a], Jiho Lee[a], Semih Akin[b], Martin Byung-Guk Jun[a]*

[a]*School of Mechanical Engineering, Purdue University, 585 Purdue Mall, West Lafayette 47907, IN, USA*
[b]*Department of Mechanical, Aerospace and Nuclear Engineering, Rensselaer Polytechnic Institute, Troy, NY 12180, USA*

* Corresponding author. Tel.: +1-765-494-3376. *E-mail address:* mbgjun@purdue.edu

Abstract

Physical Unclonable Functions (PUFs) have gained remarkable attention as a promising anti-counterfeiting solution by generating unique physical fingerprints or trust anchors derived from inherent manufacturing randomness and authenticated verification processes. Pulsed Cold Spray (PCS)—an emerging advanced manufacturing process—leverages cyclic compressed turbulent gas pulses to propel particles with high kinetic energy, enabling the creation of arbitrary patterns at each pulse that are inherently unique and physically unclonable. This study investigates the potential of PCS for generating PUFs. The gas and particle dynamics within the PCS system was analysed, and the geometry of particles at specific distances from the nozzle was visualized based on simulation results. Key parameters for achieving an optimal PUF were identified, and the simulation outcomes were validated through comparison with experimental data, confirming the conditions necessary for optimal PUF generation.

Keywords: Pulsed Cold Spray (PCS); Physical Unclonable Function (PUF); Computational Fluid Dynamics (CFD); Anti-counterfeit

1. Introduction

Preventing counterfeit goods has important implications for protecting intellectual property rights and ensuring product quality [1]. While various anti-counterfeit methods, such as holographic labels and embedded chips, have been adopted, they often involve complex manufacturing processes, leading to higher production costs and limited resistance to duplication. Physical unclonable functions (PUFs) have emerged as a promising solution, offering unreplicable physical fingerprints or trust anchors induced from inherent manufacturing randomness, which can only be authenticated through specific verification processes [2].

Among the different types of PUFs, optical PUFs leverage the unclonable physical disorder of randomly distributed materials [2]. A notable historical application occurred during the Cold War, where optical PUFs were employed in arms control by spraying a thin coating of light-reflecting particles onto the surface of nuclear weapons [2]. The random distribution of these particles produced a unique and unpredictable interference pattern when illuminated, with variations based on the viewing angle [3].

Cold Spray (CS) offers a novel approach to PUF generation by accelerating particles at supersonic velocities in turbulent flows [4]. The randomness of particle spray, combined with the resulting high kinetic energy, generates inherently unique and physically unduplicable arbitrary patterns on surfaces in each application [5]. Pulsed Cold Spray (PCS) further enhances randomness by employing cyclic compressed gas pulses to regulate gas-particle interactions [6], producing non-semantic arbitrary sparse patterns that exhibit heightened uniqueness.

This study explores the potential of employing the PCS technique for generating optical PUFs. First, the gas-particle two-phase flow and behavior of cold-sprayed particles under varying inlet pressures are analyzed by Computational

10.1016/j.procir.2025.02.269

Fluid Dynamics (CFD). Based on the numerical simulation results, parameters for optimizing PUF generation are identified. The unclonability of the optimized PUFs is then demonstrated, followed by validation through comparison with experimental results. This investigation aims to advance the development of PCS-based PUF applications and contribute to the broader field of anti-counterfeiting.

2. Methods

This study employs a twofold approach comprising simulation and experimental setups to investigate the conditions for optimal PUF generation using the PCS technique. The simulation focuses on analyzing the gas-particle dynamics and identifying key parameters, while the experimental setup validates these findings through practical application and pattern characterization.

2.1. Numerical Analysis Setup

Fig. 1 shows the three-dimensional (3D) flow domain of PCS, along with the boundary conditions used for the simulations. The modeling consists of a converging-diverging nozzle, gas inlet port, powder inlet port, and atmospheric domains. Given the time-dependent nature and supersonic compressible flows within the system, a 3D transient, turbulent, and density-based analysis was conducted using a commercial CFD package—ANSYS FLUENT 2024 R2.

The inlet gas was modeled as an ideal gas of which the specific heat is 1006.43 J/(kg-K), the molecular weight is 28.966 g/mol, the thermal conductivity was 0.0242 W/(m-K), and the viscosity is $1.7894 \cdot 10^{-5}$ kg/(m-s). Since the maximum inlet pressure of the cold spray equipment is 1.2 MPa, three CFD simulations were performed under the inlet pressures of 1.0 MPa, 1.1 MPa, and 1.2 MPa.

The discrete phase model was used to describe the behavior of feeding powders. Spherical-shaped copper (Cu) particles were used, with a total flow rate of 0.00015 kg/s. The particle size distribution, defined using the Rosin-Rammler model [7], has minimum, maximum, and mean diameters of 5 μm, 44 μm, and 36 μm, respectively. Particles were injected at a velocity of 10 m/s, perpendicular to the powder inlet surface, to minimize rebounding (see Fig. 1). Gravitational acceleration of 9.81 m/s^2 was also applied to the model.

Given the supersonic compressible flow characteristics within the pipe, the CFD simulations incorporated the Detached Eddy Simulation (DES) SST k-omega turbulence model and the Advection Upstream Splitting Method (AUSM) [8–12]. The simulation time step was set at 0.001s with 25 maximum iterations per time step.

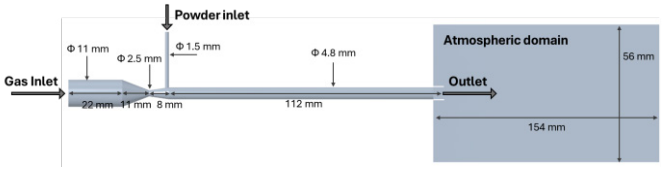

Fig. 1 Overview of 3D PCS numerical modelling

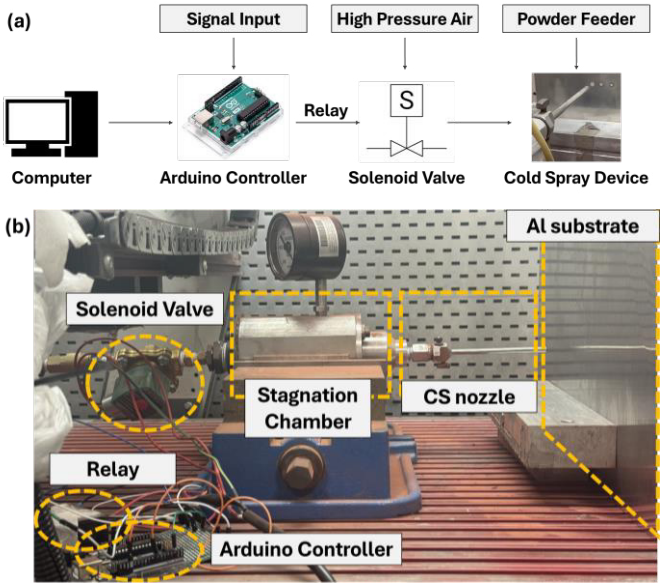

Fig. 2 PCS experimental system (a) overview, (b) setup configuration

2.2. Experimental Setup

Fig. 2 illustrates the experimental setup of the PCS system. In this setup, a computer operates an Arduino Uno controller, which activates a high-pressure solenoid valve via a high-voltage relay based on an input signal. The solenoid valve toggles on and off in 200 ms intervals, enabling programmable pulsed spraying that propels the powder toward the target surface in a controllable manner.

When the solenoid valve opens, high-pressure gas enters the PCS nozzle, pressurizing a gas expansion chamber and accelerating the gas to supersonic speeds. The high velocity creates a vacuum effect by lowering the internal pressure below atmospheric levels, thereby drawing powder from a feeder connected to the powder inlet port. This entrained powder joins the main gas flow, is further accelerated through the divergent section of the nozzle and ultimately ejected from the nozzle tip, leading to the deposition of PUFs on the target surface, where is an Aluminium (Al) plate with a thickness of 0.635 mm.

3. Results & Discussions

3.1. Powder Flow Simulation Visualization and Analysis

Fig. 3 (a) illustrates the velocity contour of the case with the inlet pressures of 1.2 MPa. The maximum velocity of the flow reaches 625 m/s (over Mach 1.8). It was observed that a more highly directional flow was formed under higher pressure conditions (see Fig. 3 (b)). Fig. 3 (c) depicts the visualization of particle positions at the cross-section located at 10, 20, 30, 40, 50, and 60 mm from the nozzle tip. The visualization was rendered at a resolution of 10,000 × 10,000 pixels, where a particle with a diameter of 5 μm was represented by a single pixel, with larger particles proportionally scaled. Only particles with velocities exceeding 300 m/s, expected to have enough kinetic energy, were included in the visualization [13]. The image was cropped at the area to 5000 x 5000 pixels from the center and resized to

1,000 × 1,000 pixels for enhanced clarity and ease of presentation. Each side of the image corresponds to 12.5 mm in actual physical size. The particle distribution was observed to become increasingly sparse with greater distances from the nozzle and lower inlet pressures.

The Scale Invariant Feature Transform (SIFT) [14] was implemented to estimate the number of descriptors in each pattern. SIFT is a computer vision algorithm designed to detect and describe local features within an image. It identifies keypoints, which are specific, distinct locations in an image, such as corners, edges, or other areas with significant texture or contrast. These keypoints are invariant to changes in scale and rotation, making them highly reliable for matching across different conditions. SIFT identifies keypoints that are invariant to scale by generating a scale space using Gaussian blurring and finding extrema in Difference-of-Gaussian (DoG) images.

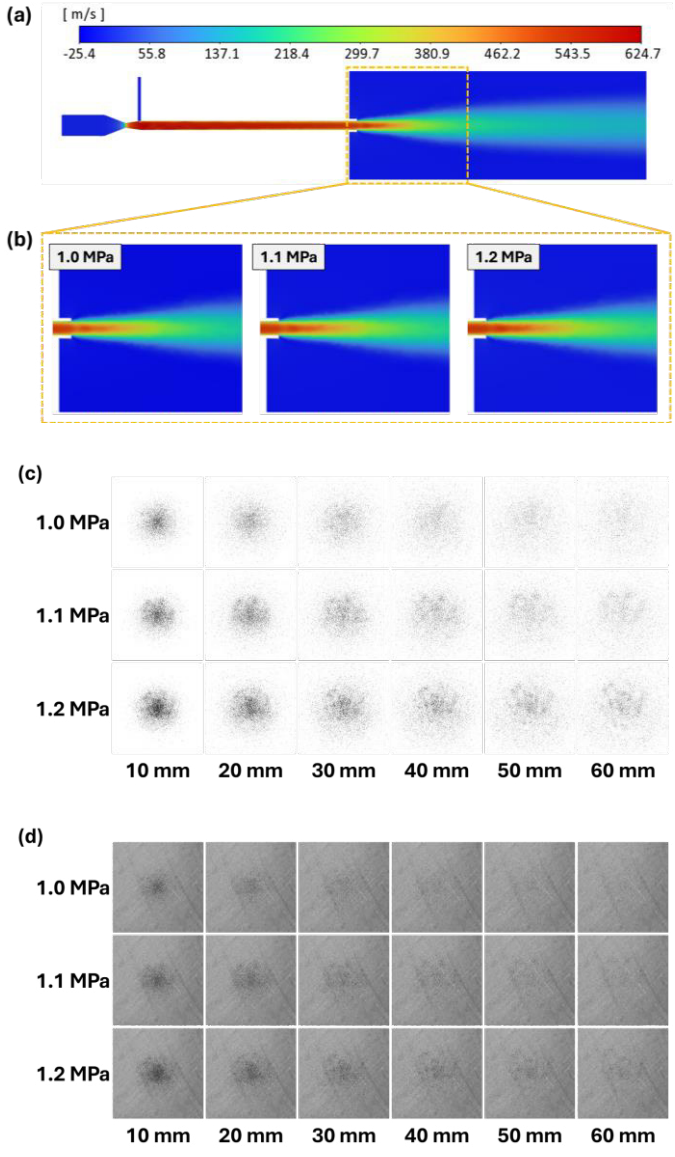

Fig. 3. (a) Velocity contour with the inlet pressures of 1.2 MPa, (b) Flows at the outlet in each pressure, (c) Visualized particles along with the distance from the nozzle tips under various pressures, (b) Integrated particle visualization to an aluminium plate surface image

Each keypoint is then characterized by a descriptor, which serves as a numerical representation of the surrounding region. Descriptors capture the gradient orientations and magnitudes within a local area, encoding detailed information about the appearance of the feature. These descriptors allow for robust pattern matching by comparing similar keypoints across images, even under variations.

By applying SIFT to the particle patterns, both the number of keypoints and their associated descriptors were quantified, enabling a detailed analysis of the distinctiveness and complexity of the patterns generated by the PCS process. This approach provided a robust foundation for evaluating the uniqueness of the patterns.

As illustrated in Fig. 4 (a), the number of keypoints increased with higher inlet pressures, reaching its maximum at a distance of 40 mm for each pressure. However, sparse patterns may be more vulnerable to noise and background interference. Fig. 3 (d) shows the integrated images overlaid onto an Al plate surface image, revealing how scratches on the plate and inherent noise from the imaging system can obstruct the extraction of keypoints. Fig. 4 (b) demonstrates the number of keypoints peaked at distances of 20–30 mm, where the pattern achieved an optimal balance between density and sparsity.

Fig. 5 presents an example of keypoint visualization at a pressure of 1.2 MPa and a distance of 40 mm for each case. SIFT extracted only half the keypoints in the overlaid image compared to the original image. Both small keypoints and the cluster's keypoint were not successfully captured in the overlaid image.

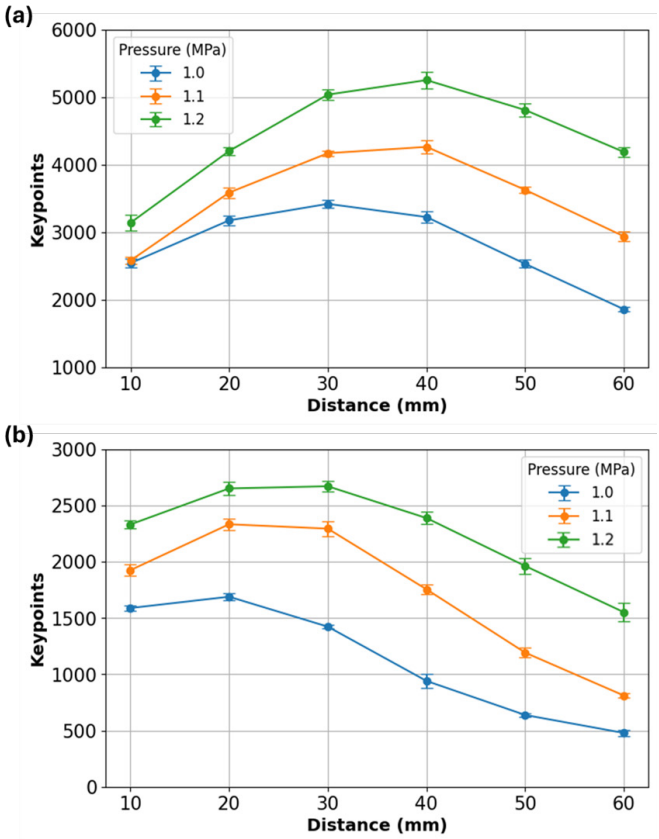

Fig. 4. The number of keypoints of (a) visualized particle images, (b) overlaid images on the plate

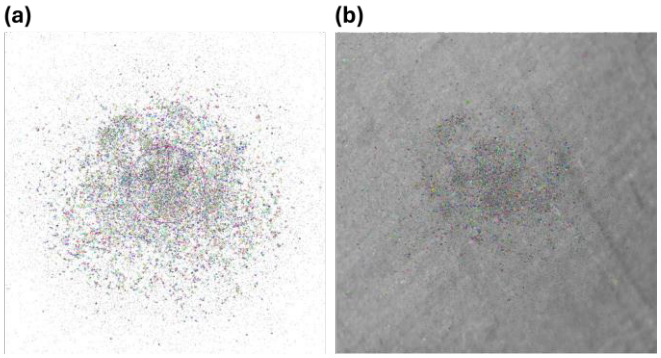

Fig. 5. Example of keypoints visualization on (a) visualized particle images (5115 keypoints), (b) overlaid images on the plate (2423 keypoints)

3.2. Uniqueness of PUFs generated by PCS

To simplify the demonstration of the uniqueness of PUFs generated by PCS, this study assumes that the positions of the pattern nodes are discrete, with a spacing of 36 μm, corresponding to the mean diameter of the powder. Within an area measuring 12.5 mm × 12.5 mm, there are totally 155,236 nodes. If PUF generation is modeled as a binary problem—where the presence of a particle is represented as 1 and its absence as 0—at least 2^{155236} unique patterns are theoretically possible.

Based on the simulation results (1.2 MPa at 30 mm), an average of 43,330 nodes were occupied by particles, allowing for at least 2^{43300} unique patterns to be generated under these conditions. This exceeds the security strength of existing encryption systems [15].

According to the simulation results, on average, 85,147 particles filled 43,330 nodes among 155,236 available. The maximum probability p, of a node being occupied by more than one particle was estimated to be 0.0164% (Fig. 6). In this scenario, each of the 85,147 particles independently occupies a given node with probability p. The probability that a specific node remains unoccupied by any particle can be approximated as follows.

$$q = (1-p)^{85147} \approx e^{-85147p} \approx 8.6 \times 10^{-7} \quad (1)$$

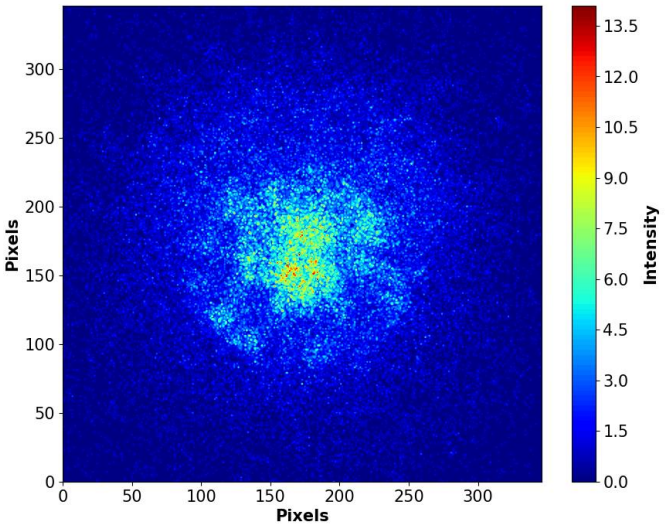

Fig. 6 Particle occupancy distribution with 1.2 MPa at 30 mm

The probability that a specific node is occupied by at least one particle is then $1-q$. If exactly 43,330 specific nodes must be occupied while the remaining 111,906 nodes remain empty, the overall probability can be expressed as:

$$(1-q)^{43330} \times q^{111906} \quad (2)$$

Since q is on the order of 10^{-7}, raising it to the power of 111,906 makes this term vanishingly small (effectively 10^{-10^6}), the overall probability extremely close to zero. Hence, this reinforces the uniqueness and security potential of the PUF patterns generated by PCS.

3.3. PUF generation and analysis

Based on the analysis, PCS patterns were generated under optimal conditions: a pressure of 1.2 MPa with plate distances of 20 mm and 30 mm, where the highest number of keypoints was observed. Patterns were created as a comparison group at a pressure of 1.1 MPa with plate distances of 20 and 30 mm.

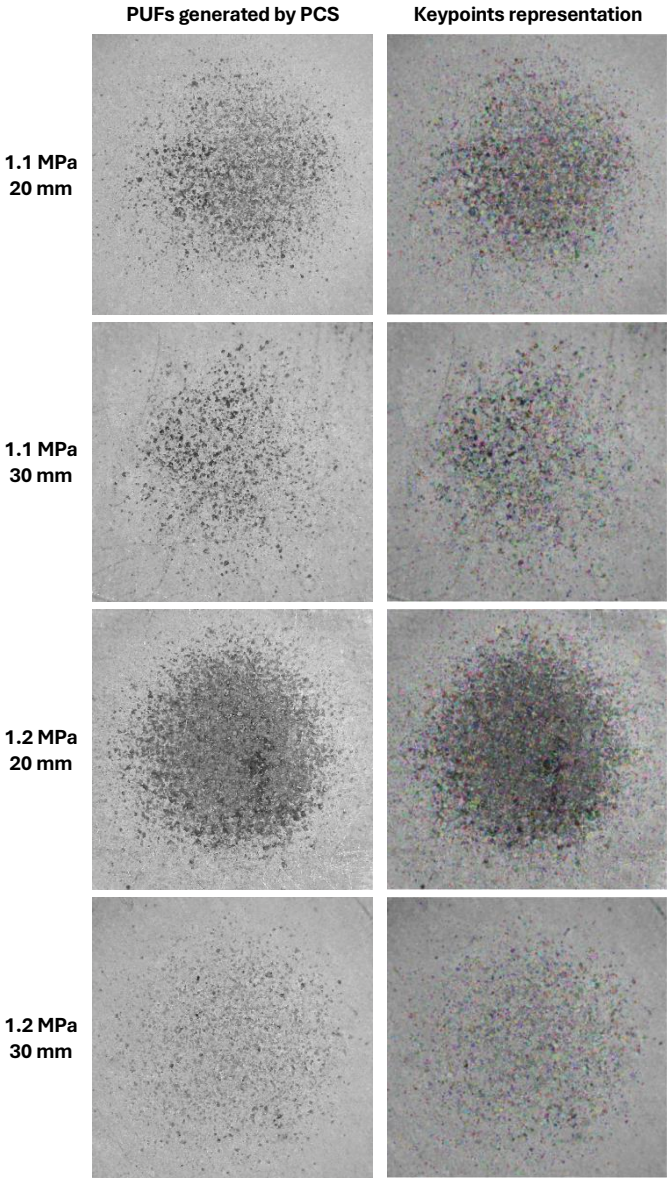

Fig. 7 PUFs generated by PCS and Keypoint representation

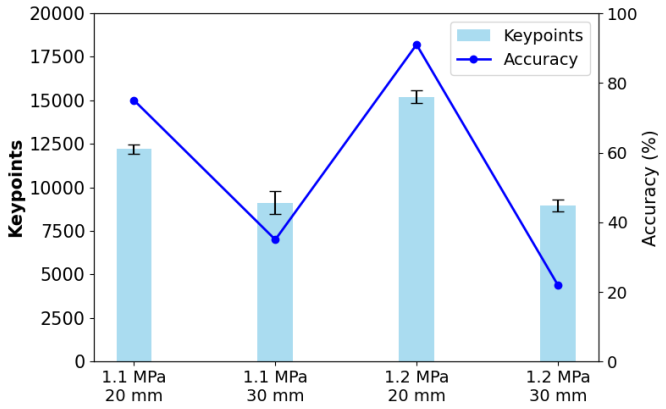

Fig. 8. The number of keypoints of the PUFs

Fig. 7 shows the generated PUFs through the PCS technique. Consistent with the simulation results, the particle distribution became progressively sparser as the distance from the nozzle increased and the inlet pressure decreased. The maximum number of keypoints was observed at a pressure of 1.2 MPa at 20 mm (Fig. 8).

SIFT matching was performed using the lowest match value among 10 reference pattern images taken at different rotation angles. Patterns were classified as identical if the match exceeded this threshold; otherwise, they were deemed different. The performance of each pattern was assessed using a dataset of 100 test images. As shown in Fig. 8, the case with the maximum number of keypoints achieved the best accuracy of 91%. However, the performance demonstrated a tendency to decline as the number of keypoints decreased.

While the number of keypoints differed by only about 20% between the cases of 1.1 MPa at 20 mm and 1.2 MPa at 20 mm, as well as 1.1 MPa at 30 mm, the accuracy of these cases showed a significant disparity of over 40%. As illustrated in Fig. 7, the cluster keypoints were successfully captured in the case of 1.1 MPa at 20 mm, but not in the other two cases. This highlights the importance of capturing the cluster's keypoints for effective pattern identification.

4. Conclusion

This study outlines the optimized parameters for the PCS technique in generating PUFs based on CFD analysis. The unclonability of the PUFs is demonstrated using probabilistic and statistical approaches. Experimental results indicate that patterns generated under the condition of 1.2 MPa at a 20 mm plate distance yield the highest number of keypoints and the greatest accuracy for identification. Given that the pattern's texture also influences uniqueness, future investigations will focus on texture creation through particle-plate collisions to enhance multi-dimensional keypoint generation. Additionally, advanced methods for pattern registration and identification will be explored to facilitate practical applications.

Acknowledgements

The authors acknowledge the support by the Manufacturing and Materials Research Laboratories (MMRL).

References

[1] Arppe R, Sørensen TJ. Physical unclonable functions generated through chemical methods for anti-counterfeiting. Nat Rev Chem 2017;1:0031. https://doi.org/10.1038/s41570-017-0031.
[2] Gao Y, Al-Sarawi SF, Abbott D. Physical unclonable functions. Nat Electron 2020;3:81–91. https://doi.org/10.1038/s41928-020-0372-5.
[3] Graybeal SN, McFate PB. Getting Out of the STARTing Block. Scientific American 1989;261:61–7.
[4] Gabor T, Akin S, Jun MB-G. Numerical studies on cold spray gas dynamics and powder flow in circular and rectangular nozzles. Journal of Manufacturing Processes 2024;114:232–46. https://doi.org/10.1016/j.jmapro.2024.02.005.
[5] Gärtner F, Stoltenhoff T, Schmidt T, Kreye H. The cold spray process and its potential for industrial applications. J Therm Spray Tech 2006;15:223–32. https://doi.org/10.1361/105996306X108110.
[6] Gabor T, Wang Y, Akin S, Zhou F, Chen J, Jeon Y, et al. Design, Modeling, and Characterization of a Pulsed Cold Spray System 2024. https://doi.org/10.2139/ssrn.5060755.
[7] Rosin, P., and Rammler. The laws governing the fineness of powdered coal. J Inst Fuel 1933;7:29–36.
[8] Liou M-S, Steffen CJ. A New Flux Splitting Scheme. Journal of Computational Physics 1993;107:23–39. https://doi.org/10.1006/jcph.1993.1122.
[9] Menter FR. Two-equation eddy-viscosity turbulence models for engineering applications. AIAA Journal 1994;32:1598–605. https://doi.org/10.2514/3.12149.
[10] Spalart PR. Comments on the Feasibility of LES for Wings and on the Hybrid RANS/LES Approach. Proceedings of the First AFOSR International Conference on DNS/LES, 1997, 1997, p. 137–47.
[11] Zhang D. Comparison of Various Turbulence Models for Unsteady Flow around a Finite Circular Cylinder at Re=20000. J Phys: Conf Ser 2017;910:012027. https://doi.org/10.1088/1742-6596/910/1/012027.
[12] Al-Rbaihat R, Saleh K, Malpress R, Buttsworth D, Alahmer H, Alahmer A. Performance evaluation of supersonic flow for variable geometry radial ejector through CFD models based on DES-turbulence models, GPR machine learning, and MPA optimization. International Journal of Thermofluids 2023;20:100487. https://doi.org/10.1016/j.ijft.2023.100487.
[13] Alkhimov AP, Papyrin AN, Kosarev VF, Nesterovich NI, Shushpanov MM. Gas-dynamic spraying method for applying a coating. US5302414A, 1994.
[14] Lowe DG. Object recognition from local scale-invariant features. Proceedings of the Seventh IEEE International Conference on Computer Vision, Kerkyra, Greece: IEEE; 1999, p. 1150–7 vol.2. https://doi.org/10.1109/ICCV.1999.790410.
[15] Barker E, Roginsky A. Transitioning the use of cryptographic algorithms and key lengths. Gaithersburg, MD: National Institute of Standards and Technology; 2019. https://doi.org/10.6028/NIST.SP.800-131Ar2.